Journal of Molecular Structure 1240 (2021) 130529

Contents lists available at ScienceDirect

Journal of Molecular Structure

journal homepage: www.elsevier.com/locate/molstr

DNA interaction, anticancer, antibacterial, ROS and lipid peroxidation studies of quinoxaline based organometallic Re(I) carbonyls

Reena R. Varma[a], Juhee G. Pandya[b], Foram U. Vaidya[c], Chandramani Pathak[c], Ravi A. Dabhi[a], Milan P. Dhaduk[a], Bhupesh S. Bhatt[a], Mohan N. Patel[a,*]

[a] Department of Chemistry, Sardar Patel University, Vallabh Vidyanagar-388 120, Gujarat, India
[b] Department of Biosciences, Sardar Patel University, Vallabh Vidyanagar, Gujarat, India
[c] Department of Cell Biology, School of Biological Sciences and Biotechnology, Indian Institute of Advanced Research, Koba Institutional Area, Gandhinagar-382007, Gujarat, India

ARTICLE INFO

Article history:
Received 1 November 2020
Revised 12 April 2021
Accepted 19 April 2021
Available online 1 May 2021

Keywords:
Organometallic Re(I) carbonyl
Cell proliferation
ROS
DNA
Cytotoxicity

ABSTRACT

Hetero mononuclear rhenium(I) complexes (I-V) using ligands (L^1-L^5) [L^1-L^5 = 11-((2-chlorobenzylidene)hydrazono)-11H-indeno[1,2-b]quinoxaline (L^1), 8-methyl-11-((4-methylbenzylidene)hydrazono)-11H-indeno[1,2-b]quinoxaline (L^2), 11-((4-bromobenzylidene) hydrazono)-8-nitro-11H-indeno[1,2-b]quinoxaline (L^3), 11-((4-bromobenzylidene) hydrazono)-8-chloro-11H-indeno[1,2-b]quinoxaline (L^4), 8-bromo-11-((4-fluorobenzylidene) hydrazono)-11H-indeno[1,2-b]quinoxaline (L^5)] were synthesized and characterized by spectroscopic method. All the synthesized compounds have biological importance. DNA interaction studies gave information about the modes of binding and the nucleolytic efficiency of compounds. The binding of the rhenium complexes to Herring sperm DNA (HS DNA) was monitored by UV–visible spectroscopy, viscosity measurements, and molecular docking studies; groove binding was suggested as the most possible mode. The DNA-complexes binding strength was measured in terms of intrinsic binding constants. *In vivo* and *In vitro* cytotoxicity against the eukaryotic and prokaryotic cells gave the toxic nature of the synthesized compounds. An antimicrobial study was carried out by estimating MIC (Minimum Inhibitory Concentration) against two Gram-positive (*S. aureus, B. subtilis*) and three Gram-negative (*S. marcescens, P. aeruginosa, E. coli)* bacteria. All synthesized complexes are biologically more active than the corresponding ligands. Complexes were having higher MDA and H_2O_2 production than ligands.

1. Introduction

The breakthrough discovery of cisplatin has accelerated bioinorganic chemistry research for the discovery of metal-based chemotherapeutic drugs with a novel mode of action [1]. The platinum-based anticancer drugs have limitations of side effects and drug resistance developed among cancer cells [2]. So, many metal-based compounds have been extensively researched for anticancer activity in search of novel compounds with potent cytotoxic nature against the cancer cell and fewer side effects [3–12]. The understanding of biomolecular interaction particularly DNA could be the most critical thing about the anticancer metallodrug discovery process since the different modes of interaction affect DNA conformation differently. Most of the metal complexes exert their antitumor activity by the metallation of DNA oligonucleotide [13].

Quinoxaline intermediates are very significant for the manufacturing of pharmaceutically active compounds [14]. Quinoxaline moiety has very wide biological applications like antibacterial [15], anticancer [16], antifungal [17], and as photochemically active materials [18]. Various antibiotics like echinomycine, levomycin, and actinoleutin contain quinoxaline rings are used for inhibiting gram +ve bacteria [19]. Many chemical and biological systems are abundant in quinoxaline moiety formed in protein and active for biological applications [20].

The carbonyl releasing ability of some metal carbonyls has been utilizing in chemotherapeutic research as an alternative to platinum-based drugs [21–24]. Also, rhenium metal is very less researched for its biological significance. So, utilizing the extensive medicinal applications of quinoxaline and CO releasing ability of metal carbonyls, we synthesized quinoxaline-based rhenium carbonyl complexes to explore their diverse biological applications.

* Corresponding authors.
E-mail addresses: bhupeshbhatt31@gmail.com (B.S. Bhatt), jeenen@gmail.com (M.N. Patel).

https://doi.org/10.1016/j.molstruc.2021.130529
0022-2860/

The interaction of Re(I) complexes with DNA was studied by UV-visible spectra, hydrodynamic volume measurement, and molecular modeling. The antibacterial and cytotoxicity studies suggest higher activity of complexes than ligands. DNA cleavage study was performed by gel electrophoresis. Synthesized complexes exhibit a good percentage of the proliferation of human carcinoma cells. Also, the ability of complexes to produce ROS and lipid peroxidation studies were carried out.

2. Experimental

2.1. Materials and methods

All the chemicals and solvents were of the reagent grade, substituted aldehyde, substituted phenylenediamine were purchased from Merck Limited (India), ninhydrin was purchased from Thirumalai Chemicals Ltd. (TCL), pentacarbonyl chloro rhenium(I) was purchased from Sigma Aldrich (USA). Luria broth, agarose, nutrient broth, and Luria broth were purchased from Himedia (India). The culture of two Gram(+ve), i.e. *Staphylococcus aureus* (*S. aureus*) (MTCC-3160) and *Bacillus subtilis* (MTCC-7193); and three Gram(-ve), i.e. *Serratia marcescens* (MTCC-7103), *Pseudomonas aeruginosa* (MTCC-1688) and *Escherichia coli* (MTCC-433), were purchased from Institute of Microbial Technology (Chandigarh, India). *S. cerevices* Var. Paul Linder 3360 was obtained from IMTECH, Chandigarh (India). HS DNA was purchased from Sigma Aldrich Chemical Co. (India).

2.2. Physical measurements

The ^{1}H and ^{13}C NMR spectra were recorded on a Bruker Avance (400 MHz). Infrared spectra were recorded on an FT–IR ABB Bomen MB 3000 spectrophotometer as KBr pellets in the range 4000–400 cm^{-1}. C, H, and N elemental analyses were performed with a Perkin–Elmer 240 elemental analyzer. Molar conductance was measured using a conductivity meter model no. EQ-660A, Mumbai (India). Melting points (°C, uncorrected) were determined in open capillaries on the ThermoCal10 melting point apparatus (Analab Scientific Pvt. Ltd, India). The electronic spectra were recorded on a UV–160A UV–Vis spectrophotometer, Shimadzu (Japan). The minimum inhibitory concentration (MIC) study was carried out using the laminar airflow cabinet (Toshiba, Delhi, India). The hydrodynamic chain length study was carried out by a viscometric measurement bath. Photo quantization of the gel after electrophoresis was carried out on AlphaDigiDocTM RT. Version V.4.0.0 PC–Image software. All density functional theory (DFT) calculations were performed using the Gaussian-09 program package.

2.3. General method for synthesis of quinoxaline based ligands (L^1-L^5)

Ligands (L^1-L^5) were obtained from the reaction between quinoxaline and Schiff base (Scheme 1). These reactions occur in two steps; the first ninhydrin reacts with different substituted phenylenediamine using water as solvent and 2 to 4 drops of H_2SO_4 as a catalyst to get indeno[1,2-b] quinoxaline derivative (3a-3e). Second, different substituted aldehyde was reacted with $NH_2NH_2.H_2O$ using two drops of H_2SO_4 as a catalyst to get substituted benzylidenehydrazine (5a-5e). Upon mixing Indeno[1,2-b] quinoxaline derivatives and benzylidenehydrazine using methanol as solvent and refluxed at 60 °C, we obtained the ligands (L^1-L^5). The ^{1}H and ^{13}C NMR spectra of all synthesized compounds are shown in supplementary material 1 and 2, respectively.

2.3.1. 11-((2-Chlorobenzylidene)hydrazono)-11H-indeno[1,2-b] quinoxaline (L1)

The synthesis was performed by taking equimolar mixture of 11H-indeno[1,2-b]quinoxalin-11-one (232 mg, 1.0 mmol) and (2-chlorobenzylidene)hydrazine (155 mg, 1.0 mmol) in 10 mL of methanol and 2 drops of H_2SO_4. Empirical formula: $C_{22}H_{13}ClN_4$; Yield: 85%; Melting point: ~192 °C; Molecular weight: 368.82 g/mol; Elemental analysis: Calc. (%): C, 71.64; H, 3.55; N, 15.19; Found (%): C, 71.62; H, 3.53; N, 15.17; Mass (m/z%): 368.80 (100) [M^+], 370.80 [M + 2]; ^{1}H NMR (400 MHz, $CDCl_3$) δ/ppm: 8.66 (1H, s, H1"a), 7.54- 8.66 (12H, m, H2,3,4,5,7,8,9,10,3″,4″,5″,6″). ^{13}C NMR (100 MHz, $CDCl_3$) δ/ppm: 163.3 (C1"c, Cquat.), 143.2 (C1′a, Cquat.), 153.8 (C5′a, Cquat.), 150.6 (C2′a, Cquat.), 150.0 (C7′a, Cquat.), 161.6 (C1"a, -CH), 143.2 (C1", Cquat.), 139.9 (C2", Cquat.), 138.5 (C10′a, Cquat.), 137.6 (C6′a, Cquat.), 133.74 (C4", −CH), 133.12 (C8, −CH), 132.1 (C3", −CH), 131.0 (C4, −CH), 130.9 (C3, −CH), 133.8 (C5, −CH), 130.0 (C2, −CH), 129.7 (C9, −CH), 129.5 (C6", −CH), 129.2 (C10, −CH), 129.1 (C5", −CH), 122.6 (C7, −CH). [Total signal observed = 22: signal of C = 9 (phenyl ring-C = 2, indeno[1,2-b]quinoxaline = 7), signal of CH = 13 (phenyl ring-CH = 4, indeno[1,2-b]quinoxaline -CH = 8, benzylidene -CH =01)]; IR (KBr, 4000–400 cm^{-1}): 3063 ν(C–H)stret., 1596 ν(C=N), 1589 ν(C-H)banding, 1428 ν(C–C)stret., 1080 ν(C-N), 810 ν(C–Cl)stret., 702 ν(Ar-H) adjacent hydrogen..

2.3.2. 8-Methyl-11-((4-methylbenzylidene)hydrazono)-11H-indeno [1,2-b]quinoxaline (L^2)

The synthesis was performed by taking equimolar mixture of 8-methyl-11H-indeno[1,2-b]quinoxalin-11-one (246 mg, 1 mmol), (4-methylbenzylidene)hydrazine (134 mg, 1.0 mmol) in 10 mL of methanol and 2 drops of H_2SO_4. Empirical formula: $C_{24}H_{18}N_4$; Yield: 68%; Melting point: ~190 °C; Molecular weight: 362.44 g/mol; Elemental analysis: Calc. (%): C, 79.54; H, 5.01; N, 15.46; Found (%): C, 79.51; H, 5.00; N, 15.44; Mass (m/z%): 362.41 (100) [M^+] ^{1}H NMR (400 MHz, $CDCl_3$) δ/ppm: 8.36 (1H, s, H1"a), 2.64 (6H,s, 2-CH_3), (7.52–8.35 (11H, m, H2,4,5,7,8,9,10,2″,3″,5″,6″). ^{13}C NMR (100 MHz, $CDCl_3$) δ/ppm: 164.5 (C1"c, Cquat.), 143.1 (C1′a, Cquat.), 153.0 (C2′a, Cquat.), 150.0 (C4'', Cquat.), 149.5 (C5′a, Cquat.), 146.8 (C7′a, Cquat), 161.1 (C1"a, −CH), 143.0 (C3, Cquat.), 139.3 (C1", Cquat.), 138.5 (C10′a, Cquat.), 136.8 (C6′a, Cquat.), 130.3 (C3",5″, −CH), 130.0 (C2",6″, −CH), 129.7 (C4, −CH), 129.0 (C8, −CH), 124.2 (C10, −CH), 122.4 (C9, −CH), 122.2 (C5, −CH), 122.1 (C2, −CH), 120.6 (C7, −CH), 21.7 (-CH_3), 21.9 (-CH_3). [Total signal observed = 22: signal of C = 10 (phenyl ring-C = 2, indeno[1,2-b]quinoxaline = 8), signal of CH = 10 (phenyl ring-CH = 2, indeno[1,2-b]quinoxaline -CH = 7, benzylidene -CH =01, CH_3 = 02)]; IR (KBr, 4000–400 cm^{-1}): 3063 ν(C–H)stret., 1604 ν(C=N), 1588 ν(C-H)banding, 1488 ν(C–C)stret., 1087 ν(C-N), 815 ν(p-substisution), 701 ν(Ar-H) adjacent hydrogen.

2.3.3. 11-((4-Bromobenzylidene)hydrazono)-8-nitro-11H-indeno[1,2-b] quinoxaline (L^3)

The synthesis was performed by taking equimolar mixture of 8-nitro-11H-indeno[1,2-b]quinoxalin-11-one (277 mg, 1.0 mmol), (4-bromobenzylidene)hydrazine (199 mg, 1.0 mmol) in 10 mL of methanol and 2 drops of H_2SO_4. Empirical formula: $C_{22}H_{12}BrN_5O_2$; Yield: 83%; Melting point: ~198 °C; Molecular weight: 458.28 g/mol; Elemental analysis: Calc. (%): C, 57.66; H, 2.64; N, 15.28; Found (%): C, 57.64; H, 2.62; N, 15.25; Mass (m/z%): 458.26 (100) [M^+], 460.26 [M + 2] ^{1}H NMR (400 MHz, $CDCl_3$) δ/ppm: 9.28 (1H, s, H1"a), 7.42- 9.27 (11H, m, H2,4,5,7,8,9,10,2″,3″,5″,6″). ^{13}C NMR (100 MHz, $CDCl_3$) δ/ppm: 163.6 (C1"c, Cquat.), 160.8 (C6′a, Cquat.), 153.3 (C2′a, Cquat.), 138.2 (C1′a, Cquat.), 149.7 (C5′a, Cquat.), 147.4 (C3, Cquat.), 141.87 (C7′a, Cquat.), 139.5 (C1", Cquat.), 138.8 (C10′a, Cquat.), 150.0 (C1''a, -CH), 137.5 (C4", Cquat.), 133.9 (C3",5″, −CH), 133.6 (C8, −CH),

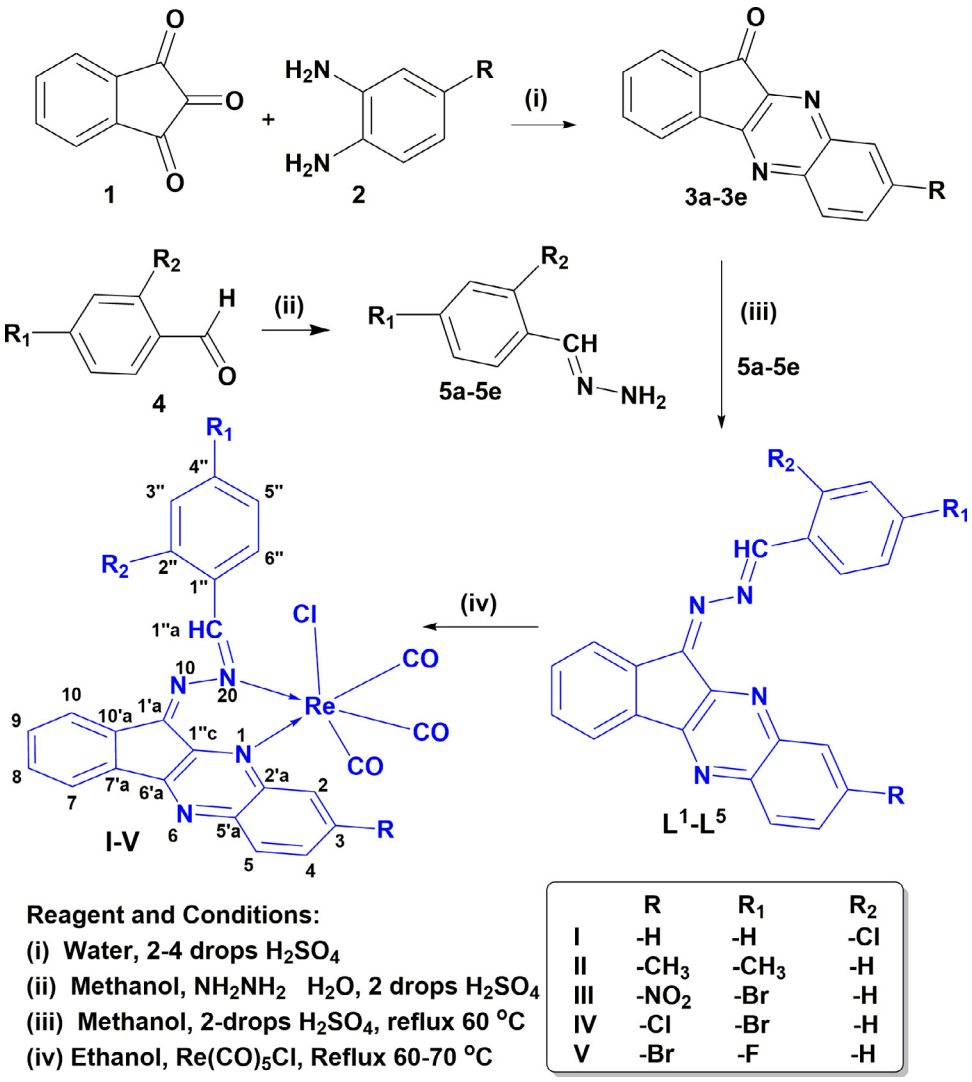

	R	R_1	R_2
I	-H	-H	-Cl
II	$-CH_3$	$-CH_3$	-H
III	$-NO_2$	-Br	-H
IV	-Cl	-Br	-H
V	-Br	-F	-H

Scheme 1. General scheme for the synthesis of ligands (L^1-L^5) and complexes (I-V).

133.3 (C9, −CH), 131.0 (C10, −CH), 129.8 (C2",6″, −CH), 127.6 (C5, −CH), 126.6 (C7, −CH), 125.6 (C2, −CH), 123.4 (C4, −CH). [Total signal observed = 20: signal of C = 10 (phenyl ring-C = 2, indeno[1,2-b]quinoxaline = 8), signal of CH = 10 (phenyl ring-CH = 2, indeno[1,2-b]quinoxaline -CH = 7, benzylidene -CH =01)]; IR (KBr, 4000–400 cm^{-1}): 3078 ν(C–H)stret., 1651 ν(C=N), 1630 ν(C-H)banding, 1589 ν(C–C)stret., 1527 ν(presence of $-NO_2$), 1040 ν(C-N), 818 ν(p-substisution), 733 ν(Ar-H) adjacent hydrogen, 618 ν(C-Br).

2.3.4. 11-((4-Bromobenzylidene)hydrazono)-8-chloro-11H-indeno[1,2-b]quinoxaline (L^4)

The synthesis was performed by taking equimolar mixture of 8-chloro-11H-indeno[1,2-b]quinoxalin-11-one (267 mg, 1.0 mmol), (4-bromobenzylidene)hydrazine (199 mg, 1.0 mmol) in 10 mL of methanol and 2 drops of H_2SO_4. Empirical formula: $C_{22}H_{12}BrClN_4$; Yield: 83%; Melting point: ~194 °C; Molecular weight: 447.72 g/mol; Elemental analysis: Calc. (%): C, 59.02; H, 2.70; N, 12.51; Found (%): C, 59.00; H, 2.68; N, 12.49; Mass (m/z%): 447.70 (100) [M^+], 449.70[M + 2], 451.70 [M + 4]; ^{1}H NMR (400 MHz, $CDCl_3$) δ/ppm: 8.58 (1H, s, H1"a), 7.32- 8.58 (11H, m, H2,4,5,7,8,9,10,2″,3″,5″,6″). ^{13}C NMR (100 MHz, $CDCl_3$) δ/ppm: 163.9 (C1"c, Cquat.), 142.7 (C1′a, Cquat.), 153.4 (C2′a, Cquat.), 150.3 (C3, Cquat.), 150.0 (C5′a, Cquat.), 146.6 (C7′a, Cquat.), 162.2 (C1"a, -CH), 142.2 (C1", Cquat.), 139.9 (C10′a, Cquat.), 138.2 (C6′a, -CH), 137.3 (C3",5″, Cquat.), 136.7 (C4", Cquat,), 135.9 (C4, −CH), 134.2 (C8, −CH), 131.0 (C5, −CH), 130.7 (C10, −CH), 130.1 (C9, −CH), 127.7 (C2",6″, −CH), 126.4 (C7, −CH), 125.3 (C2, −CH). [Total signal observed = 20: signal of C = 10 (phenyl ring-C = 2, indeno[1,2-b]quinoxaline = 8), signal of CH = 10 (phenyl ring-CH = 2, indeno[1,2-b]quinoxaline -CH = 7, benzylidene -CH =01)]; IR (KBr, 4000–400 cm^{-1}): 3032 ν(C–H)stret., 1651 ν(C=N), 1612 ν(C-H)banding, 1597 ν(C–C)stret., 1042 ν(C-N), 818 ν(p-substisution), 724 ν(C–Cl)stret., 720 ν(Ar-H) adjacent hydrogen, 632 ν(C-Br).

2.3.5. 8-Bromo-11-((4-fluorobenzylidene)hydrazono)-11H-indeno[1,2-b]quinoxaline (L^5)

The synthesis was performed by taking equimolar mixture of 8-bromo-11H-indeno[1,2-b]quinoxalin-11-one (311 mg, 1.0 mmol), (4-fluorobenzylidene)hydrazine (138 mg, 1.0 mmol) in 10 mL of methanol and 2 drops of H_2SO_4. Empirical formula: $C_{22}H_{12}BrFN_4$; Yield: 87%; Melting point: ~200 °C; Molecular weight: 431.27 g/mol; Elemental analysis: Calc. (%): C, 61.27; H, 2.80; N, 12.99; Found (%): -; Mass (m/z%): 450.46 (100) [M+]; ^{1}H NMR (400 MHz, $CDCl_3$) δ/ppm: 8.41 (1H, s, H1"a), 7.55- 8.40 (11H,

m, H2,4,5,7,8,9,10,2″,3″,5″,6″). ^{13}C NMR (100 MHz, $CDCl_3$) δ/ppm: 164.3 (C4", Cquat.), 162.9 (C1′'c, Cquat.), 143.4 (C1′a, Cquat.), 151.0 (C5′a, Cquat.), 150.0 (C2′a, Cquat.), 147.1 (C7′a, Cquat.), 154.1 (C1"a, -CH), 143.1 (C1", Cquat.), 139.9 (C10′a, Cquat.), 138.6 (C6′a, Cquat.), 137.9 (C2, -CH), 137.7 (C3, Cquat,), 135.8 (C8, −CH), 134.7 (C4, −CH), 132.8 (C2",6″, −CH), 130.7 (C5, −CH), 130.0 (C10, −CH), 128.2 (C9, −CH), 126.6 (C7, −CH), 125.5 (C3",5″, −CH). [Total signal observed = 20: signal of C = 10 (phenyl ring-C = 2, indeno[1,2-b]quinoxaline = 8), signal of CH = 10 (phenyl ring-CH = 2, indeno[1,2-b]quinoxaline -CH = 7, benzylidene -CH =01)]; IR (KBr, 4000–400 cm^{-1}): 3032 ν(C–H)stret., 1651 ν(C=N), 1612 ν(C-H)banding, 1597 ν(C–C)stret., 1042 ν(C-N), 818 ν(p-substisution), 722 ν(C–Cl)stret., 720 ν(Ar-H) adjacent hydrogen, 635 ν(C-Br)stret.

2.4. General synthesis of complexes (I-V)

The precursor of $[Re(CO)_5Cl]$ in ethanol was refluxed for 10 min with continuous stirring at ambient conditions. In the solution, the ethanolic solution of ligand (L^{1-} L^5) was poured to get a yellowish-green solution at the primary stage. The reaction mixture was refluxed at 60–70 °C temperature for 10 h in inert atmosphere [25,26]. The completion of the reaction was checked using a silica-coated TCL plate (ethyl acetate and hexane). The crude was filtered to remove solid particles. The solvent was removed under reduced pressure to obtain the brownish-red product (Scheme 1).

2.4.1. Synthesis of $[Re(CO)_3(L^1)Cl]$ (I)

The synthesis was performed by taking equimolar mixture of $Re(CO)_5Cl$ (361 mg, 1.0 mmol) and ligand (L^1) (369 mg, 1.0 mmol). Empirical formula: $C_{25}H_{13}C_{l2}N_4O_3Re$; Yield: 81%; Melting point: ~392 °C; Molecular weight: 674.51 g/mol; Elemental analysis: Calc. (%): C, 44.52; H, 1.94; N, 8.31;Re, 27.61; Found (%): C, 44.50; H, 1.95; N, 8.28; Re, 27.58; Conductance: 2.97 $ohm^{-1}cm^2mol^{-1}$; ^{1}H NMR (400 MHz, DMSO-d_6) δ/ppm: 8.74 (1H, s, H1"a), 7.61- 8.74 (12H, m, H2,3,4,5,7,8,9,10,3″,4″,5″,6″). ^{13}C NMR (100 MHz, DMSO-d_6) δ/ppm: 186.3 (2M-CO, Cquat.), 183.3 (M-CO, Cquat.), 165.1 (C1"c, Cquat.), 142.2 (C1′a, Cquat.), 154.5 (C5′a, Cquat.), 152.2 (C2′a, Cquat.), 151.0 (C7′a, Cquat.), 163.3 (C1"a, -CH), 143.3 (C1", Cquat.), 140.0 (C2", Cquat.), 139.4 (C10′a, Cquat.), 138.0 (C6′a, Cquat.), 134.1 (C4", −CH), 133.5 (C8, −CH), 132.7 (C3", −CH), 131.5 (C4, −CH), 131.3 (C3, −CH), 131.0 (C5, −CH), 130.6 (C2, −CH), 130.5 (C9, −CH), 130.0 (C6", −CH), 129.9 (C10, −CH), 129.7 (C5", −CH), 123.5 (C7, −CH). [Total signal observed = 24: signal of C = 11 (M-CO = 2, phenyl ring-C = 2, indeno[1,2-b]quinoxaline = 7), signal of CH = 13 (phenyl ring-CH = 4, indeno[1,2-b]quinoxaline -CH = 8, benzylidene -CH =01)]; IR (KBr, 4000–400 cm^{-1}): 3063 ν(C–H)stret., 1596 ν(C=N), 1589 ν(C-H)banding, 1428 ν(C–C)stret., 1080 ν(C-N), 817 ν(C–Cl)stret., 702 ν(Ar-H) adjacent hydrogen.

2.4.2. Synthesis of $[Re(CO)_3(L^2)Cl]$ (II)

The synthesis was performed by taking equimolar mixture of $Re(CO)_5Cl$ (361 mg, 1.0 mmol) and ligand (L^2) (362 mg, 1.0 mmol). Empirical formula: $C_{27}H_{18}ClN_4O_3Re$; Yield: 84%; Melting point: ~388 °C; Molecular weight: 668.12 g/mol; Elemental analysis: Calc. (%): C, 48.54; H, 2.72; N, 8.39; Re, 27.87; Found (%): C, 48.52; H, 2.69; N, 8.37; Re, 27.86; Conductance: 5.72 $ohm^{-1}cm^2mol^{-1}$; ^{1}H NMR (400 MHz, DMSO-d_6) δ/ppm: 8.34 (1H, s, H1"a), 2.69 (6H,s, 2-CH_3), 7.61- 8.34 (11H, m, H2,4,5,7,8,9,10,2″,3″,5″,6″). ^{13}C NMR (100 MHz, DMSO-d_6) δ/ppm: 185.5 (2M-CO, Cquat.), 182.4 (M-CO, Cquat.), 165.4 (C1"c, Cquat.), 144.6 (C1′a, Cquat.), 154.8 (C2′a, Cquat.), 152.8 (C4′', CH), 152.3 (C5′a, Cquat.), 148.2 (C7′a, Cquat.), 163.5 (C1"a, −CH), 144.1 (C3, Cquat.), 140.0 (C1", Cquat.), 140.0 (C10′a, Cquat.), 138.1 (C6′a, Cquat.), 132.4 (C3",5″, −CH), 132.2 (C2",6″, −CH), 130.0 (C4, −CH), 130.0 (C8, −CH), 126.3 (C10, −CH), 124.6 (C9, −CH), 124.4 (C5, −CH), 124.3 (C2, −CH), 122.6 (C7, −CH), 22.4 (-CH_3), 22.2 (-CH_3). [Total signal observed = 24: signal of C = 12 (M-CO = 2, phenyl ring-C = 2, indeno[1,2-b]quinoxaline = 8), signal of CH = 10 (phenyl ring-CH = 2, indeno[1,2-b]quinoxaline -CH = 7, benzylidene -CH =01), -CH_3 = 02]; IR (KBr, 4000–400 cm^{-1}): 3063 ν(C–H)stret., 1604 ν(C=N), 1588 ν(C-H)banding, 1488 ν(C–C)stret., 1087 ν(C-N), 815 ν(p-substisution), 701 ν(Ar-H) adjacent hydrogen.

2.4.3. Synthesis of $[Re(CO)_3(L^3)Cl]$ (III)

The synthesis was performed by taking equimolar mixture of $Re(CO)_5Cl$ (361 mg, 1.0 mmol) and ligand (L^3) (458 mg, 1.0 mmol). Empirical formula: $C_{25}H_{12}BrClN_5O_5Re$; Yield: 85%; Melting point: ~ 392 °C; Molecular weight: 763.96 g/mol; Elemental analysis: Calc. (%): C, 39.30; H, 1.58; N, 9.17; Re, 24.37; Found (%): C, 39.28; H, 1.56; N, 9.15; Re,24.35; Conductance: 10.12 $ohm^{-1}cm^2mol^{-1}$; ^{1}H NMR (400 MHz, DMSO-d_6) δ/ppm: 9.29 (1H, s, H1"a), 7.56- 9.29 (11H, m, H2,4,5,7,8,9,10,2″,3″,5″,6″). ^{13}C NMR (100 MHz, DMSO-d_6) δ/ppm: 188.8 (2M-CO, Cquat.), 185.2 (M-CO, Cquat.), 165.5 (C1"c, Cquat.), 164.4 (C6′a, Cquat.), 154.6 (C2′a, Cquat.), 139.3 (C1′a, CH), 151.6 (C5′a, Cquat.), 148.5 (C3, Cquat.), 143.3 (C7′a, Cquat.), 140.0 (C1", Cquat.), 139.5 (C10′a, Cquat.), 152.8 (C1′'a, -CH), 137.8 (C4", Cquat.), 135.6 (C3",5″, −CH), 135.2 (C8, −CH), 135.1 (C9, −CH), 132.2 (C10, −CH), 130.0 (C2",6″, −CH), 128.3 (C5, −CH), 126.8 (C7, −CH), 126.2 (C2, −CH), 124.7 (C4, −CH). [Total signal observed = 22: signal of C = 12 (M-CO = 2, phenyl ring-C = 2, indeno[1,2-b]quinoxaline = 8), signal of CH = 10 (phenyl ring-CH = 2, indeno[1,2-b]quinoxaline -CH = 7, benzylidene -CH =01)]; IR (KBr, 4000–400 cm^{-1}): 3078 ν(C–H)stret., 1651 ν(C=N), 1630 ν(C-H)banding, 1589 ν(C–C)stret., 1527 ν(presence of -NO_2), 1040 ν(C-N), 818 ν(p-substisution), 625 ν(C-Br), 733 ν(Ar-H) adjacent hydrogen.

2.4.4. Synthesis of $[Re(CO)_3(L^4)Cl]$ (IV)

The synthesis was performed by taking equimolar mixture of $Re(CO)_5Cl$ (361 mg, 1.0 mmol) and ligand (L^4) (448 mg, 1.0 mmol). Empirical formula: $C_{25}H_{12}BrCl_2N_4O_3Re$; Yield: 79%; Melting point: ~388 °C; Molecular weight: 753.41 g/mol; Elemental analysis: Calc.(%): C, 39.86; H, 1.61; N, 7.44; Re, 24.72; Found (%): C, 39.84; H, 1.58; N, 7.41; Re,24.68; Conductance: 4.15 $ohm^{-1}cm^2mol^{-1}$; ^{1}H NMR (400 MHz, DMSO-d_6) δ/ppm: 8.62 (1H, s, H1"a), 7.25- 8.62 (11H, m, H2,4,5,7,8,9,10,2″,3″,5″,6″). ^{13}C NMR (100 MHz, DMSO-d_6) δ/ppm: 187.2 (2M-CO, Cquat.), 185.1 (M-CO, Cquat.), 165.4 (C1"c, Cquat.), 144.5 (C1′a, Cquat.), 154.5 (C2′a, Cquat.), 152.7 (C3, Cquat.), 151.4 (C5′a, Cquat.), 148.6 (C7′a, Cquat.), 163.5 (C1"a, -CH), 144.2 (C1", Cquat.), 141.4 (C10′a, Cquat.), 139.9 (C6′a, -CH), 138.4 (C3",5″, Cquat.), 138.1 (C4", Cquat,), 136.6 (C4, −CH), 135.2 (C8, −CH), 133.8 (C5, −CH), 133.3 (C10, −CH), 132.2 (C9, −CH), 129.6 (C2",6″, −CH), 127.5 (C7, −CH), 126.5 (C2, −CH). [Total signal observed = 22: signal of C = 12 (M-CO = 2, phenyl ring-C = 2, indeno[1,2-b]quinoxaline = 8), signal of CH = 10 (phenyl ring-CH = 2, indeno[1,2-b]quinoxaline -CH = 7, benzylidene -CH =01)]; IR (KBr, 4000–400 cm^{-1}): 3032 ν(C–H)stret., 1651 ν(C=N), 1612 ν(C-H)banding, 1597 ν(C–C)stret., 1042 ν(C-N), 818 ν(p-substisution), 725 ν(C–Cl)stret., 720 ν(Ar-H) adjacent hydrogen, 640 ν(C-Br).

2.4.5. Synthesis of $[Re(CO)_3(L^5)Cl]$ (V)

The synthesis was performed by taking equimolar mixture of $Re(CO)_5Cl$ (361 mg, 1.0 mmol) and ligand (L^5) (431 mg, 1.0 mmol). Empirical formula: $C_{25}H_{12}BrClFN_4O_3Re$; Yield: 81%; Melting point: ~395 °C; Molecular weight: 736.96 g/mol; Elemental analysis: Calc. (%): C, 40.75; H, 1.64;N, 7.60; Re, 25.27; Conductance: 18.88 $ohm^{-1}cm^2mol^{-1}$; ^{1}H NMR (400 MHz, DMSO-d_6) δ/ppm: 8.65 (1H, s, H1"a), 8.01- 8.64 (11H, m, H2,4,5,7,8,9,10,2″,3″,5″,6″). ^{13}C NMR (100 MHz, DMSO-d_6) δ/ppm: 190.0(2M-CO, Cquat.), 188.1 (M-CO, Cquat.), 166.4 (C4", Cquat.), 164.5 (C1′'c, Cquat.), 144.8

(C1′a, Cquat.), 153.8 (C5′a, Cquat.), 152.5 (C2′a, Cquat.), 149.0 (C7′a, Cquat.), 155.6 (C1"a, -CH), 144.3 (C1", Cquat.), 140.0 (C10′a, Cquat.), 139.9 (C6′a, -CH), 138.1 (C2, -CH), 137.9 (C3, Cquat,), 136.8 (C8, −CH), 135.5 (C4, −CH), 132.8 (C2",6′′, −CH), 133.4 (C5, −CH), 131.5 (C10, −CH), 129.1 (C9, −CH), 127.2 (C7, −CH), 126.8 (C3",5′′, −CH). [Total signal observed = 22: signal of C = 12 (M-CO = 2, phenyl ring-C = 2, indeno[1,2-b]quinoxaline = 8), signal of CH = 10 (phenyl ring-CH = 2, indeno[1,2-b]quinoxaline -CH = 7, benzylidene -CH =01)]; IR (KBr, 4000–400 cm^{-1}): 3071 ν(C–H)stret., 1651 ν(C=N), 1612 ν(C-H)banding, 1597 ν(C–C), 1150 ν(C-F), 1049 ν(C-N), 818 ν(p-substisution), 741 ν(Ar-H) adjacent hydrogen, 640 ν(C-Br).

2.5. Antiproliferation study

Stock solutions of 10–100 mg/mL test complexes (I-V) were prepared in dimethyl sulfoxide (DMSO). HCT 116 cells were cultured in RPMI 1640 medium. The culture media were supplemented with 10% fetal bovine serum and an antibiotic cocktail containing penicillin (5 mg/mL), streptomycin (5 mg/mL), and neomycin (10 mg/mL). The cells were cultured in a humidified atmosphere of 5% CO_2 at 37 °C. The entire study was executed using exponentially growing cells. Twenty-four hours after cell plating, media was removed and replaced with fresh media containing 10, 25, 50, 100, 500 μg/mL test compounds and DMSO as vehicle control for the indicated exposure times. The Re(I) tricarbonyl complexes I-V were tested for their *in vitro* cytotoxicity against colon carcinoma (HCT116) cancerous cell lines by the MTT (3-(4,5-dimethylthiazol-2-yl)-2,5-diphenyltetrazolium bromide) assay. The extent of inhibition was displayed as an IC_{50} value, which is the concentration required to inhibit cell growth to half [27].

2.6. Cellular level bioassay using S. cerevisiae cells

The cellular level bioassay was carried out using *S. cerevisiae* cells [28]. The cells were grown in 50 mL yeast extract media in a 150 mL Erlenmeyer flask. The flask was incubated at 30 °C on a shaker at 150 rpm till the exponential growth of *S. cerevisiae* was obtained (24 to 30 h). The cell culture was treated with different concentrations (2, 4, 6, 8, 10 mg/mL) of complexes, free ligands, and DMSO (control), and incubated for 16–18 h. The next day, the treated cells were collected by centrifugation at 10,000 rpm for 10 min and were dissolved in 500 mL of PBS. The 80 mL of yeast culture dissolved in PBS and 20 mL of 0.4% trypan blue prepared in PBS were mixed, and cells were observed in a compound microscope (40X). The dye could enter the dead cell only, so they appeared blue whereas live cells resisted the entry of dye. The number of dead cells and the number of live cells were counted.

2.7. Brine shrimp lethality bioassay

The cytotoxicity of complexes was studied on brine shrimp, *Artemia cysts*, according to the reported method [29]. In this experiment, 10 nauplii (larvae) were added to the vials of 24-well Microtiter plate with a total volume of to 2500 µL per vial [1450 µL sea salt solution + 1000 µL sea salt containing 10 nauplii + 50 µL (complex + DMSO)], [DMSO] <2% (V/V). After 24 h of incubation, live and dead larvae were counted and the LC_{50} values were determined for each complex [30].

2.8. In vitro antibacterial screening

The *in vitro* antibacterial activity of ligands and complexes was performed according to the literature procedure [31]. Luria Broth was used as the bacteria growth medium. Serially diluted concentrations of each of test compounds (in DMSO) from 20 to 2800 µM were prepared for the determination of MIC and vaccinated with five different microorganisms. The solution without turbidity was noted as the minimum inhibitory concentration after overnight incubation at 37 °C.

2.9. Reactive oxygen species (ROS)

The amount of H_2O_2 was quantified as described by Loreto and Velikova [32]. In the process, treated culture centrifuged at 5000 rpm for 5 min, was used for H_2O_2 determination. The reaction system consists of 0.5 mL supernatant was added to 0.5 ml of 10 mM phosphate buffer (pH 7.0) and 1.0 mL of 1 M KI. After completion of the reaction, absorbance was measured at 390 nm and results were expressed as µg/mL H_2O_2 of culture.

2.10. Lipid peroxidation

For the measurements of lipid peroxidation in *Saccharomyces cerevisiae*, the thiobarbituric acid (TBA) test, which determines MDA as an end product of lipid peroxidation (Heath and Parker, 1968) [33], was used. We combined 1.0 mL of biological sample {0.1–2.0 mg of membrane protein or 0.1–0.2 /µmol of lipid phosphate} with 2.0 mL of TCA-TBA-HCI and mixed it thoroughly. The solution was heated for 15 min in a boiling water bath. After cooling, the flocculent precipitates were removed by centrifugation at 1000 rpm for 10 min. The absorbance of the sample was determined at 535 nm against a blank that contains all the reagents minus the lipid. The malondialdehyde concentration of the sample was calculated using an extinction coefficient of 1.56 × 10 ~ M^{-1} cm^{-1} [34].

2.11. DNA interaction

2.11.1. Absorption spectral analysis

The change in spectral behavior of the complex upon interacting with DNA is a tool for determining the interaction of complexes. The extent of the spectral shift of complexes in the presence of DNA reveals the affinity and nature of binding [35]. In the experiment, a fixed amount of DNA solution (100 μL) in phosphate buffer was added to sample cell holding the definite concentration of the complex solution (20 μmol/L) and reference cell to nullify the effect of HS DNA, and allowed to incubate for 10 min before the spectra being recorded. DMSO was also added into the reference cell as a control to nullify the effect of DMSO [36].

2.11.2. Hydrodynamic volume or viscosity measurement

Viscometric experiments were performed using an Ubbelohde viscometer, maintained at 25.0 (±0.5)°C in a thermostatic water bath. The total system was a 3 mL solution of DNA, buffer, and the increasing concentration of compounds. The concentration of DNA was 100 μM and that of metal complex was varied from 5 to 50 μM. The flow time of solutions in phosphate buffer (pH 7.0) was recorded in triplicate for each sample, and an average flow time was calculated. Data were presented as $(\eta/\eta^0)^{1/3}$ versus [Compound]/[DNA], where η is the viscosity of DNA in the presence of complex and η^0 is the viscosity of DNA alone. The hydrodynamic length of DNA generally increases upon partial intercalation while it does not lengthen upon groove binding [37].

2.11.3. Molecular docking with DNA sequence d(ACCGACGTCGGT)$_2$

Docking study was measured for Re(I) complexes with deoxyribonucleic acid (DNA). The main purpose of molecular docking is to identify the binding mode of metal complexes using Hex 8.0 software according to the reported procedure [38].

2.11.4. Agarose gel electrophoresis

The effect of compounds on the integrity of DNA of *S. cerevisiae* cells results of cytotoxicity encouraged us to find out whether the compounds have any effect on the integrity of DNA. DNA extraction of *S. cerevisiae* yeast given in the literature [39]. Gel electrophoresis of plasmid DNA (*S. cerevisiae* DNA) was carried out in 0.8% agarose gel containing 2.5 μL100mM ethidium bromide (EtBr) in 50 ml TAE buffer (0.4 gm agarose in 50 ml TAE buffer) submerge the gel in electrophoresis. Mix the appropriate amount of isolated DNA with gel and load the mixture (5μL Dye + 3μL sample DNA) mix it properly then load into the gel. Apply a voltage of 100 Volt, DNA will migrate towards positive anodes, when DNA sample or dye have migrated a sufficient distance turn off the power to analyze the gel in UV-light. Image of gel observed in instrument AlphaDigiDoc^{TM} RT. Version V.4.0.0 PC–Image software. The effect of the complexes (I-V) on the DNA integrity of *S. cerevisiae* was carried out by the isolation of DNA from treated and untreated *S. cerevisiae* cells and electrophoresed on 1% agarose gel followed by visualization.

3. Results and discussion

3.1. Characterization

The compounds were characterized by ^{1}H NMR, ^{13}C (APT) NMR, IR, mass, electronic spectra, elemental analysis and conductivity measurement. The characterization data supports the proposed structure of Re(I) complexes. We have also performed theoretical calculations (DFT study) for Re(I) complexes to further support the proposed structure of Re(I) complexes. The single crystal XRD of similar type of compounds are reported in the literature [26,40].

The ^{1}H NMR of ligands L^1-L^5 demonstrate peak at 7.53- 8.65 δ ppm, 7.52- 8.35 δ ppm, 7.42–9.27 and 7.56- 9.29 δ ppm, 7.32–8.58 δ ppm, and 7.55- 8.40 δ ppm. In the complexes (I-V), these peaks are shifted to 7.61–8.7 δ ppm, 7.61–8.34 δ ppm, 7.56–9.29 δ ppm, 7.25–8.62 δ ppm, and 8.01–8.64 δ ppm, respectively. In addition to above data, there is down field shifting occurs for the proton H1''a after complexation i.e., 8.65 to 8.74 in L^1, 8.36 to 8.34 in L^2, 9.28 to 9.29 in L^3, 8.58 to 8.62 in L^4 and 8.41 to 8.65 in L^5. The change in chemical shift values is observed for two carbon atoms i.e., C-1''a and C-1'a, among these two carbon atoms C-1''a shows more shifting as compared to C-1'a after complexation. Down field shifting for C-1''a are 161.6 to 163.3 in L^1, 161.1 to 163.5 in L^2, 150.0 to 152.8 in L^3, 162.2 to 163.5 in L^4 and 154.1 to 155.6 in L^5. These change in chemical shift for H-1''a and more down field shift for C-1''a than C-1'a suggest that coordination occurs from N-20 atom. ^{13}C-APT data of ligand L^1-L^5 and complexes (I-V) show signals at 126.0–166.0 δ ppm, which are assigned to the aromatic carbon. In APT spectra, quartet and methylene carbon exhibited normal signals, while -CH and $-CH_3$ signals are inverted. Signals at 180.0–195.0 δ ppm value are assigned to carbonyl groups forming a covalent bond with the metal ion.

The FT-IR spectra of quinoxaline based ligands (L^1-L^5) and complexes I -V demonstrate the signal for quinoxaline ring contain ν(C=N) extending groups at 1600 – 1650 cm^{-1} range. The signal at 1500- 1625 cm^{-1} is assigned for C–C stretching, while signals at ~640 cm^{-1}, ~817 cm$^{-1,}$ and ~1150 cm^{-1} are assigned to C-Br, C–Cl and C-F stretching. Each complex indicates (-CO) signal at around 2030–1860 cm^{-1}, typical of a pseudo-C_3v symmetry resulting from a facial arrangement of carbonyls [41]. The magnetic moments (μ_{eff}) value of rhenium(I) is found zero, indicate it does not have unpaired electron (low spin t_2g^6 eg^0 configuration) i.e. all the rhenium(I) complexes are diamagnetic with +1 oxidation state of rhenium metal ion. IR spectroscopic data of Re(I) complexes suggest that all three CO in $Re(CO)_3$ have shown its characteristic band between 1735 and 2021 cm^{-1} [42], it gives the confirmation of all bounded CO in rhenium(I) metal complexes. Observed frequencies for metal coordinated CO ligands are lower than free CO ligands i.e., 2143 cm^{-1} [43]. CO-stretching frequency data proved that CO group involves in back-bonding (metal/CO p-back donation into the p* CO orbital), it decreases the bond strength of CO ligands and ultimately increases the bond strength of Re-CO bond.

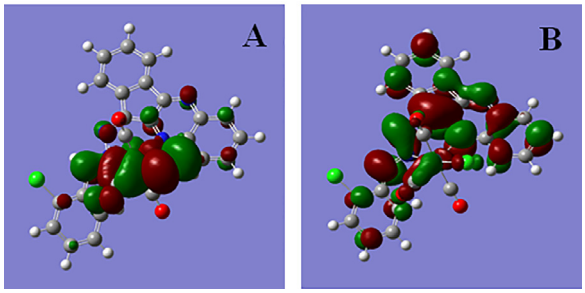

Fig. 1. HOMO (A) and LUMO (B) orbital containing structures of the complex - I.

The Λm (molar conductance) values of complexes (I-V) were found in the range of 2.00 – 18.88 Ω^{-1}cm^{2}mol^{-1}. It suggests that complexes (I-V) are non-ionic and chemically neutral.

The electronic spectra of the synthesized ligands (L^1-L^5) and complexes (I- V) were recorded at ambient conditions in DMSO. Two bands appeared in the electronic spectrum: MLCT (metal to ligand charge transfer) band at 332–400 nm region and LMCT (ligand to metal charge transfer) band at 240–330 nm region. The bands are characteristics of the octahedral environment of ligands around Re(I) metal ion [44].

3.2. Computational analysis

All density functional theory (DFT) calculations were performed using the Gaussian-09 program package. The DFT/B3LYP (Becke three-parameter Lee-Yang-Parr) method with LanL2DZ basis set is used to determine optimized geometry in which bond lengths and bond angles are calculated. The optimized electronic structure, optimized bond length and bond angles of all complexes are shown in supplementary material 3.

3.2.1. Homo-Lumo energy

The frontier molecular orbitals (FMO), HOMO, and LUMO play a significant role in the study of electrical and optical properties. The HOMO (highest occupied molecular orbital) and LUMO (lowest unoccupied molecular orbital) give information about the interaction of a molecule with other species. The HOMO signifies the ability to donate an electron, and the LUMO to accept an electron. A molecule with a small difference in the orbital energy is usually more reactive. Among numerous other uses, the energy gap (Eg) between HOMO and LUMO is used to predict the activity and intramolecular charge transfer in organic as well as inorganic molecules with conjugated π bonds. The energy gap between HOMO-LUMO orbitals of the complexes I - V are 1.8251 eV, 1.8648 eV, 1.7878 eV, 1.8022 eV, and 1.8240 eV, respectively in the gaseous phase. From Fig. 1, it can be concluded that HOMO is evenly distributed in the central Re atom through the carbonyl group whereas LUMO is distributed in the ligand's moiety. HOMO-LUMO orbital structures of all the complexes are shown in supplementary material 3.

3.2.2. Mulliken population analysis

The atomic charge can be determined by Mulliken population analysis (MPA) of the complexes. The bonding ability of a molecule depends on the electronic charge on the atoms. The analysis of complex-I expresses that the atoms Cl28

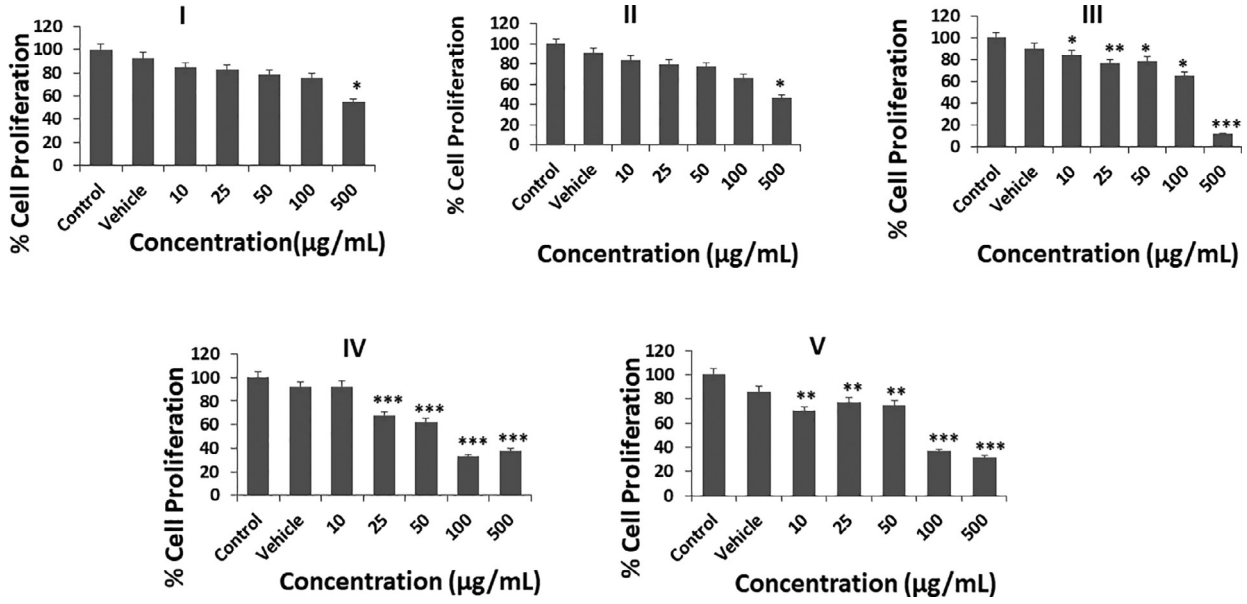

Fig. 2. % Cell proliferation of complexes (I-V).

(−0.247047), C26 (−0.25944), N19 (−0.182141), N (−0.202768) display highest electronegativity and atoms C4 (0.441342), C5 (0.409261), C21 (0.47035), Re27 (0.411185) display highest electropositivity. In complex-II, the atoms C7 (−0.332792), C9 (−0.268581), N14 (−0.20396), N20 (−0.205225), Cl30 (−0.25974) and O32(−0.172988) display highest electronegativity and atoms C4 (0.439819), C5(0.41042), C17(0.44617), C22(0.444474), C25 (0.454096), Re29 (0.424837) show highest electropositivity. In complex-III, the atoms C7 (−0.318857), C9 (−0.266415), N14 (−0.206599), N19 (−0.202071), Cl28 (−0.22399), O48 (−0.233999) show highest electronegativity and atoms C4 (0.439741), C5 (0.419576), C17 (0.347119), C21 (0.452091), Re27 (0.421684) show highest electropositivity. In complex-IV, the atoms C7 (−0.32735), C9 (−0.26432), N14 (−0.20268), N19 (−0.2054), C24 (−0.20677), Cl28 (−0.24086) show highest electronegativity and atoms C4 (0.439861), C5 (0.412316), C13 (0.227544), C21 (0.453369), Re27 (0.422756) show highest electropositivity. In complex-V, the atoms C7 (−0.329007), C9 (−0.263397), N14 (−0.203263), C17 (−0.301049), N19 (−0.202252), Cl28 (−0.241002), F47 (−0.223174) show highest electronegativity and atoms C4 (0.440203), C5 (0.411233), C13 (0.221772), C21 (0.458317), C24 (0.347367), Re27 (0.420536) show highest electropositivity. All the values and bar-chart analysis of Mulliken charges for all complexes are shown in the supplementary material 3.

3.3. Antiproliferation study

Synthesized complexes (I-V) were tested for cell antiproliferation activity by MTT assay on the HCT 116 cell line. The% cell proliferation decreased with an increase in complex concentration due to inhibition of tumor cells. The decreasing order of IC_{50} values is cisplatin> oxaliplatin > IV > V > carboplatin > III > I > II (Fig. 2). Above 500 μg/mL concentration, the solution becomes turbid, and coloration occurred. The IC_{50} values of synthesised complexes (I-V) and standard drugs cisplatin, carboplatin, oxaliplatin are >500 μg/mL, >500 μg/mL, 465.2 μg/mL, 60.9 μg/mL, 77.10 μg/mL, 15.49 μg/mL, >111.37 μg/mL, and 22.66 μg/mL, respectively. The results suggest that complex-IV is most cytotoxic, and we can say that our approach to synthesize metal complexes having carbon monoxide (CO) and heterocyclic compound chelated with rhenium metal is promising in terms of enhancing anticancer activity.

3.4. Cellular level bioassay using S. cerevisiae

The cellular level cytotoxicity of ligands L^1-L^5 and complexes I-V was carried out by using *Saccharomyces Cerevisiae* cells in terms of% viability (Supplementary material 4). The *in vitro* toxicity was found to vary with the concentrations of the synthesized compounds, chelating ligands environment, and CO ligand directly linked by a synergic bond with Re(I) metal ion. The increase in compound concentration resulted in a decrease in% cell viability. Amongst all ligands, L^5 is most potent as it contains the most electronegative F-atom at *p*-position to the ancillary ligand, while L^2 is least potent as it contains electron-donating -CH_3 group. All complexes have higher%viability (more potent) than all ligands. At 40.75 μg/mL concentration, complex-V showed maximum cytotoxicity as it is having fluorine substituted ligand. The increasing order of%viability of ligands and complexes are V > IV > III > I > II >L^5 >L^4 >L^3 > L^1 > L^2.

3.5. In vivo brine shrimp lethality bioassay (BSLB)

The BSLB method was used for calculating the%mortality and toxic nature of synthesized compounds in terms of the death of the larvae. A plot of the log of the sample's concentration versus percentage (%) of mortality showed a linear correlation. The synthesized ligands have more mortality rate as compared to the synthesized complexes. The increasing order of mortality rate of ligands and complexes is L^1 (13.94 μg/mL) < L^2 (12.12 μg/mL) < L^3 (12.10 μg/mL) < L^4 (12.05 μg/mL) < L^5 (9.85 μg/mL) < *I* (20.21 μg/mL) < II (20.03 μg/mL) < III (18.05 μg/mL) < IV (16.22 μg/mL) < *V* (16.06 μg/mL). From the graph, LC_{50} values (shown in brackets) of the compounds were calculated, ligand L^5 is most cytotoxic due to the presence of F-atom and L^2 has the least cytotoxicity (due to electron-donating methyl group) amongst ligands. Furthermore, all complexes are more cytotoxic than ligands. The complex-V is the most potent as it is having the most electronegative and smallest in size F-atom containing ligand. All compounds have higher cytotoxicity than reported Pd(II) complexes [45], and $[PtCl_2(L^6)]$ [46].

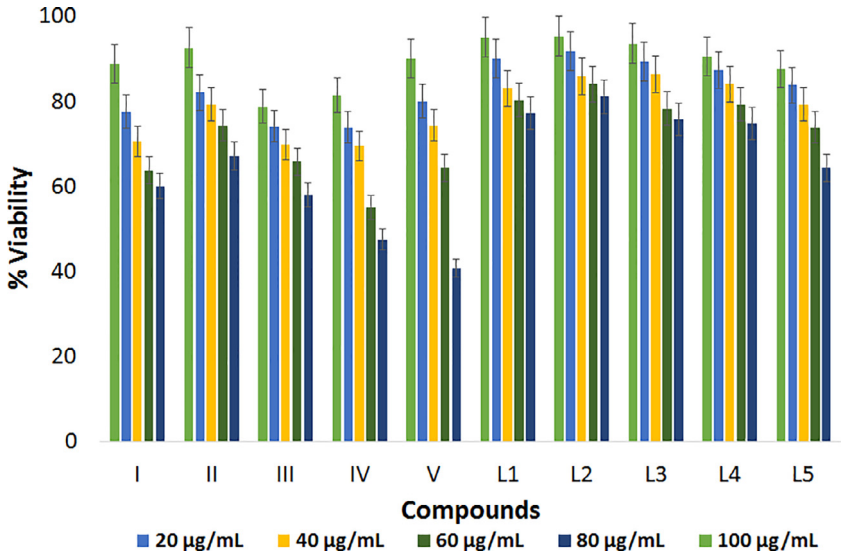

Fig. 3. % Cell viability of ligands (L^1-L^5) and complexes (I-V).

3.6. In vitro *antibacterial screening*

The synthesized heterocyclic ligands (L^1-L^5) and the complexes (I-V) were tested against two Gram +ve (*S. aureus, B. subtilis*) and three Gram -ve (*S. marcescens, P. aeruginosa, E. coli)* bacteria. The data reveals that all complexes have a greater inhibition rate of bacteria than neutral bidentate ligands (L^1-L^5) and a metal salt (Supplementary material 5). For the synthesized complexes, two factors are applicable, the ligands that are bound to metal ions in a multidentate fashion, and the nature of the ligand [47]. The MIC values of the complexes and ligands are observed in the range of 60–90 μM, and 280–320 μM (Supplementary material 5), respectively; which are comparable to the reported rhenium(I) complexes (MIC = 16–256 μM) [48]. Complex-V and III are the most active amongst all the compounds. The increasing order of MIC values is $L^2 < L^1 < L^3 < L^4 < L^5 <$ II < IV < *I* < III < *V*. Bulkiness and electronegativity affects the MIC values. Amongst all ligands, L^2 has a higher MIC value (least potent) due to presence of electron donating methyl group and L^5 has least MIC value (more potent) due to presence of most electronegative F-atom to the ancillary ligand. All metal complexes have lower MIC values (more potent) than ligands. The complex-V has the least MIC value (most potent) due to the presence of F-atom substituted ligand.

3.7. *Reactive oxygen species (ROS)*

The lethal effect of synthesized ligands (L^1-L^5) and complexes (I- V) on growth inhibition of *Saccharomyces cerevisiae* was evaluated by quantification of H_2O_2, as ROS. Here we found that treated cells were showing greater production of H_2O_2, as compared to untreated cells. The H_2O_2 concentration was increasing with increasing the test sample concentration (Supplementary material 6). The decreasing order of H_2O_2 accumulation is as V > IV > III > I > II > L^5 >L^4 >L^3 > L^1 > L^2 (Fig. 3). The results state that complexes show a higher toxic effect than ligands, and the ROS generation rate depends upon compounds concentration and functionality on compounds. This was further confirmed by observing their effects on the DNA integrity of *Saccharomyces cerevisiae* as higher H_2O_2 causes DNA damage. Metabolic processes in cells produce reactive oxygen species (ROS) i.e., oxygen-derived molecules such as hydrogen peroxide (H_2O_2), superoxide anion ($O_2^{\bullet-}$), and hydroxyl radical (•OH) [49]. The presence of reactive oxygen species in the cell is very harmful to the DNA and leads to cancer. The synthesized compounds can react with ROS, and thus convert ROS to hydrogen peroxide. The H_2O_2 might have contradictory effects on cell proliferation depending on the concentration and cell type, it may cause an antiproliferative effect [50]. The reaction of metal complexes with ROS produces higher H_2O_2 accumulation than ligands that leads to cell death. So, it can be concluded that metal complexes are more cytotoxic than ligands as H_2O_2 accumulation is greater in treated cells (death cells) than untreated cells. The higher production of H_2O_2 indicates more effectiveness of compounds to inhibit the production of ROS.

3.8. *Lipid peroxidation*

Pure lipid suspensions and liposomes can improve metal-based autoxidation, which produces malondialdehyde that reacts with lipid tissue to form lipofuscin, thus reducing its concentration in the cell. Therefore, MDA concentration involves peroxidation in biological membranes. There are three ways of autoxidation; the first is free-radical-based oxidation, the second is without free radial nonenzymatic oxidation and the third is autooxidation in the presence of enzymes. Lipid contains tissues like fatty acids and excess cholesterol in the heart that are oxidized by ROS techniques and decrease its content in the tissue. Production of MDA concentration increased with time and concentration, it was time- concentration dependent method. The results state that the MDA content was higher in complexes than the ligands. So, the toxic nature of complexes was higher than the ligands (Fig. 4) (Supplementary material 7). The decreasing order of MDA concentration is V > IV > III > I > II >L^5 >L^4 >L^3 > L^1 > L^2. The compounds containing electronegative fluorine atom as substituent have the highest activity, while compounds containing electron-donating methyl group possess the least activity. The ligand L^5 stimulates the production of MDA concentration most effectively, while ligand L^2 is the least effective in the production of MDA concentration. Furthermore, all complexes exhibit higher MDA concentration than the ligands. The complex-V is the most effective in stimulating the production of MDA.

3.9. *DNA interactions*

3.9.1. *Absorption titration*

The binding mode and binding constant (K_b) of the complexes toward DNA gives an idea about the strength of interaction, which

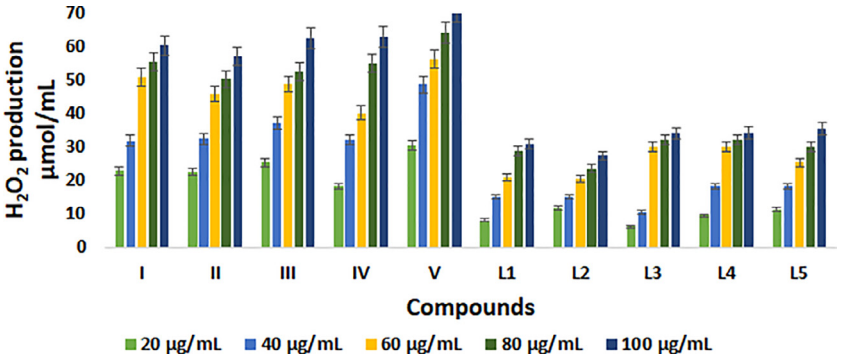

Fig. 4. H_2O_2 accumulation of ligands (L^1-L^5) and complexes (I-V).

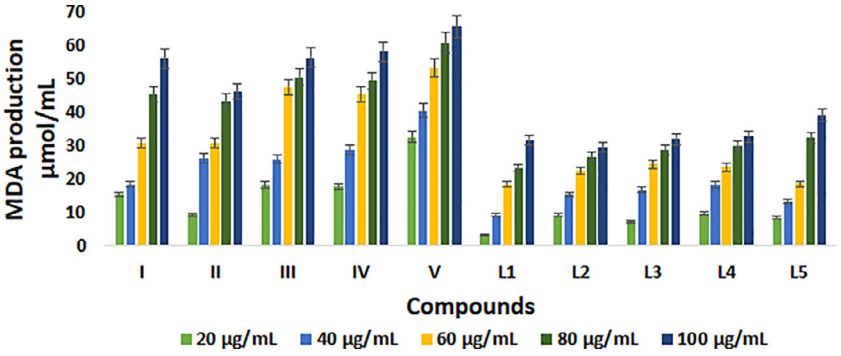

Fig. 5. MDA production in *S. cerevisiae* yeast using ligands (L^1-L^5) and complex (I-V).

can be obtained by studying UV–vis. absorption spectra. The successive addition of DNA (100 μL) to the fixed concentration of complexes at 10 min break time resulted in a decrease in absorption (hypochromism) and a small redshift. It suggests that all complexes (I-V) bind to DNA through major or minor groove results [35]. The binding constant (K_b) values were estimated from the plot of [DNA]/(ε_a-ε_f) versus [DNA] concentration, the slope to intercept ratio value gives binding constant K_b value (Fig. 5). The absorption spectral changes were monitored at around 240–330 nm for the investigation of the DNA binding mode and strength. The decreasing order of binding constant (shown in brackets) is V (2.6×10^5 M^{-1}) > IV (2.3×10^5 M^{-1}) > II (1.9×10^5 M^{-1}) > I (1.8×10^5 M^{-1}) > III (1.1×10^5 M^{-1}) > L^4 (0.9×10^5 M^{-1}) > L^3 (0.8×10^5 M^{-1}) > L^1 (0.6×10^5 M^{-1}) > L^2 (0.4×10^5 M^{-1}) > L^5 (0.3×10^5 M^{-1}). All complexes show higher binding constant values than the ligands. Complex-V containing electronegative fluorine atom as a substituent to the ancillary ligand exhibit the highest binding strength towards DNA. The synthesized compounds possess higher binding strength than reported Re(I) complexes (K_b = 7.95 (±1.89) × 10^4 M^{-1}) [42]. The K_b value of all complexes are comparable with the reported rhodium(III) and iridium(III) complexes (K_b = 1.94 × 10^5 –3.12 × 10^5 M^{-1}) [51].

3.9.2. Hydrodynamic volume or viscosity measurement

Viscosity measurements of DNA solution were carried out by varying the concentration of compounds to get an idea of the binding mode. Groove binding causes less pronounced or only a minor change in the viscosity [52]. The experimental values were plotted as $(\eta/\eta^0)^{1/3}$ v/s [complex]/[DNA] and [ligand]/[DNA] (Supplementary material 8). The ability to decrease the $(\eta/\eta^0)^{1/3}$ of complexes is in order V > IV > I > II > III > L^2 > L^3 > L^1 > L^5 > L^4. Complexes show a higher $(\eta/\eta^0)^{1/3}$ value than ligands, which was also supported by reported compounds [53]. The complex-V has the highest $(\eta/\eta^0)^{1/3}$ value. The EB (ethidium bromide) shows the intercalation mode of binding, which increase the viscosity of DNA. While the effect was less pronounced in the case of synthesized compounds, which showed a slight increase in viscosity of DNA similar to minor groove binder netropsin [54,55]. These show that compounds are more likely to have DNA groove binding mode [44,55].

3.9.3. Molecular docking with DNA sequence d(ACCGACGTCGGT)$_2$

Molecular docking study gives the idea of the orientation of ligands and complexes inside the DNA groove [56,57]. The complexes (I- V) and ligands (L^1-L^5) are shown by the ball and stick and DNA base pairs are shown by the licorice model using Hex 8.0 software. The structure of ligands and complexes were drawn in .CDX format using ChemBioDraw Ultra 14.0, then converted to PDB format using Chem3D (Cambridge Soft). For docking studies, the structural coordinates of DNA were obtained from the protein data bank (pdb id: 423D) [58]. Re(I) complexes bind to base-pair A–T, C–G, G–C, A–T (B-DNA) at minor grooves of the DNA (Fig. 6) (Supplementary material 9). Docking energies of ligands (L^1-L^5) and complexes (I-V) are −268.84 kJ/mol, −270.95 kJ/mol, −281.54 kJ/mol, −277.15 kJ/mol, −277.65 kJ/mol, −283.75 kJ/mol, −280.82 kJ/mol, −302.12 kJ/mol, −288.47 kJ/mol, −290.23 kJ/mol, respectively. Complex III shows higher negative binding energy (−302.12 KJ/mol) than the other complexes and ligands. The ascending order of energy is L^1 < L^2 < L^4 < L^5 < L^3 < II < I < IV < V < III.

3.9.4. Effect of compounds on the DNA of S. cerevisiae cells

The Agarose gel electrophoresis technique was used to check the DNA cleavage efficiency of ligands (L^1-L^5) and complexes (I-V) [59]. The electrophoretic separation of *S. cerevisiae* DNA upon treatment with compounds under aerobic conditions suggests that complexes (I-V) have much higher binding efficacy to the *S. cerevisiae* DNA than the quinoxaline based ligands (L^1-L^5). Ligands show lesser smearing as compared to the complexes (Fig. 7). It suggests that DNA cleavage efficiency complexes are higher than

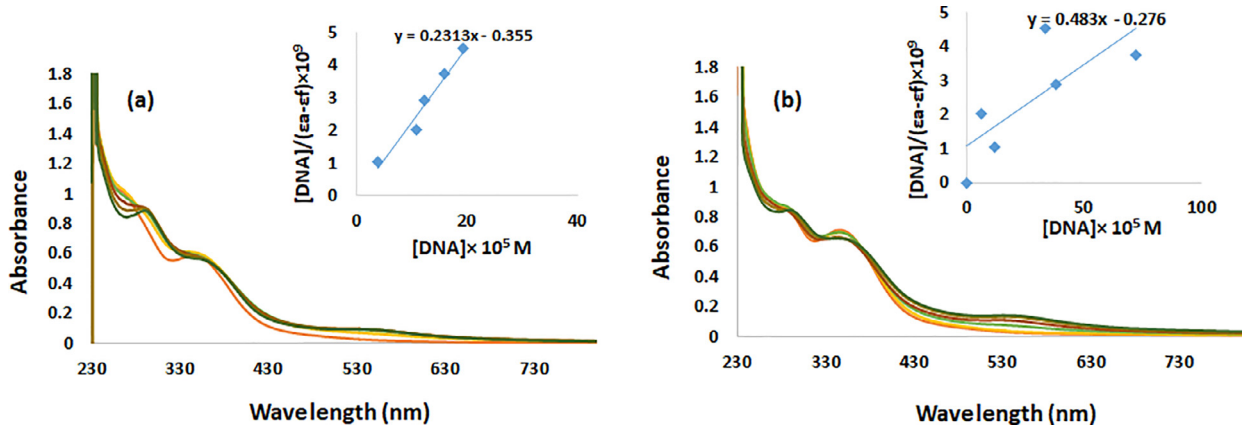

Fig. 6. UV–visible spectra of (a) ligand (L^1) and (b) complex-I.

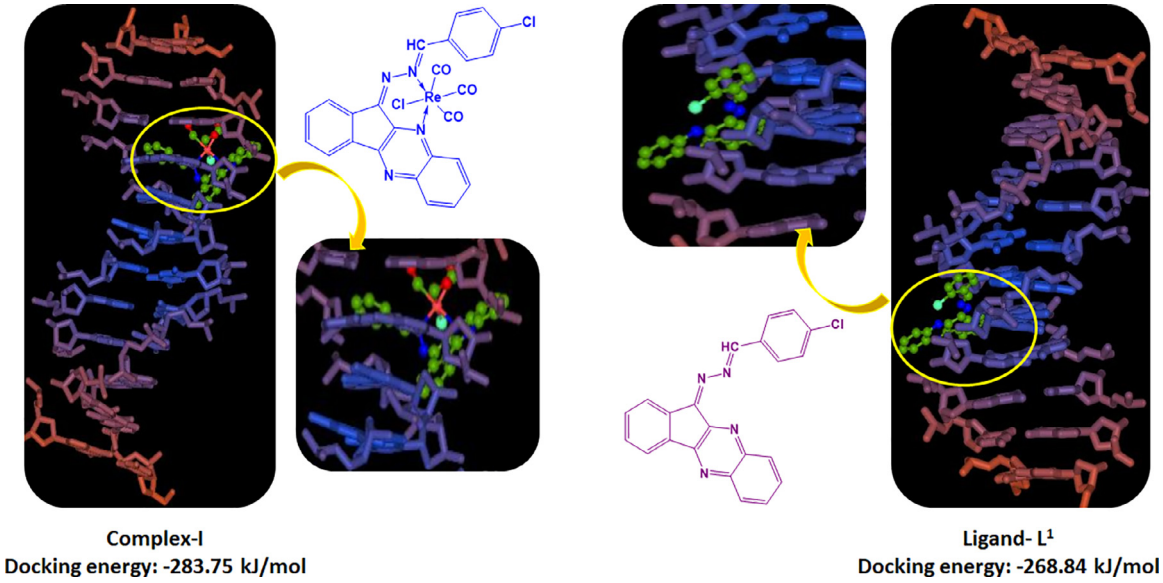

Fig. 7. Molecular docking of ligand (L^1) and complex (I) by the ball and stick model and DNA by VDW sphere.

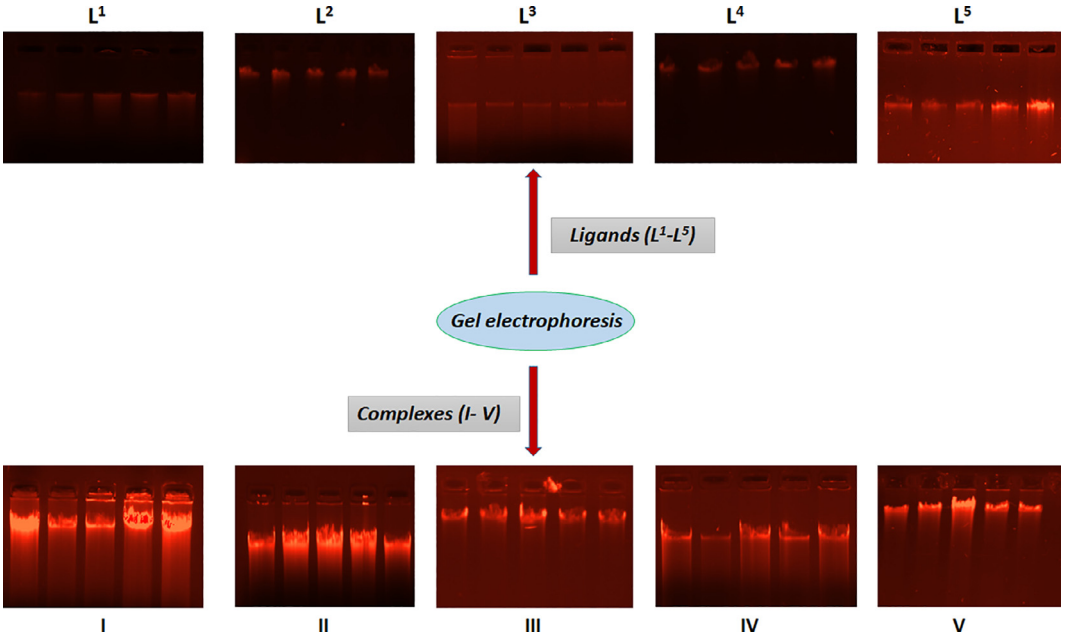

Fig. 8. Electrophoretic cleavage of S. cerevisiae DNA using ligands (L1-L5) and complexes (I-V).

the ligands. Complexes-V, I, and II show a better cleavage effect of DNA, complex-III show moderate cleavage effect of DNA and complex-IV shows lesser cleavage effect on DNA.

4. Conclusions

A series of substituted quinoxaline based organometallic rhenium(I) complexes were synthesized and well-characterized, in search of new organometallic complexes that can show better antibacterial, cytotoxicity, reactive oxygen species production, lipid peroxidation, genotoxicity, DNA binding, and DNA cleavage activities. The synthetic approach was carried out by pentacarbonyl chloro rhenium(I) as the starting material for preparing the novel neutral organometallic complexes having octahedral structure and diamagnetic. ^{1}H NMR and ^{13}C NMR data concluded that coordination occurs through N-20 atom and resultant complex have six membered chelate ring. The DFT calculations were performed for estimation of bond length and bond angle data, theoretically. The Mulliken charge analysis of complexes by DFT studies was performed for the evaluation of atomic charge in complexes. The HOMO-LUMO molecular energy diagram and energy gap determination by DFT calculation show the charge distribution in complexes. DNA binding study was carried out by absorption titration, viscosity measurement, and molecular modeling. Binding constant (K_b) values of complexes were higher than the ligands, it shows the higher binding capability of complexes with DNA i.e., groove binding. There was a minor change in the viscosity in complexes than the ethidium bromide suggests DNA groove binding of complexes. In molecular modeling, docking energies of complexes were found higher than the ligands. The presence of a more electronegative environment improves the antibacterial activity as suggested by MIC data. Complex-IV was observed most antiproliferative than all synthesized compounds, cisplatin, oxaliplatin, and carboplatin. All the complexes showed well *in vitro* cytotoxic, cellular level bioassay, reactive oxygen species production, and lipid peroxidation compared to ligands. The ability to produce reactive oxygen species and lipid peroxidation may be the reason for the good antiproliferative activity of complexes.

Quinoxaline based organometallic rhenium(I) complexes were synthesized and screened for diverse biological activities such as anticancer, antibacterial, *in vivo* and *in vitro* cytotoxicity, DNA interaction, ROS production and lipid peroxidation. Some compounds have better biological activities than standard drugs.

Declaration of Competing Interest

The authors declare no conflict of interest.

CRediT authorship contribution statement

Reena R. Varma: Investigation, Conceptualization, Writing – original draft, Formal analysis, Methodology. **Juhee G. Pandya:** Investigation, Conceptualization, Formal analysis. **Foram U. Vaidya:** Investigation, Conceptualization, Formal analysis. **Chandramani Pathak:** Writing – review & editing, Supervision. **Ravi A. Dabhi:** Writing – review & editing, Software. **Milan P. Dhaduk:** Writing – review & editing, Software. **Bhupesh S. Bhatt:** Writing – review & editing, Formal analysis. **Mohan N. Patel:** Conceptualization, Writing – original draft, Supervision, Writing – review & editing.

Acknowledgement

The authors are thankful to the Head, Department of Chemistry, Sardar Patel University, Vallabh Vidyanagar, Gujarat, India, for providing necessary research facilities, Sardar Patel University, Vallabh Vidyanagar, CPEPA, UGC, New Delhi for providing chemicals facility, DST-PURSE Sardar Patel University, Vallabh Vidyanagar for LC-MS analysis.

Supplementary materials

Supplementary material associated with this article can be found, in the online version, at doi:10.1016/j.molstruc.2021.130529.

References

[1] T. Lazarević, A. Rilak, Ž.D. Bugarčić, Platinum, palladium, gold and ruthenium complexes as anticancer agents: current clinical uses, cytotoxicity studies and future perspectives, Eur. J. Med. Chem. 142 (2017) 8–31.
[2] A.-M. Florea, D. Büsselberg, Cisplatin as an anti-tumor drug: cellular mechanisms of activity, drug resistance and induced side effects, Cancers 3 (1) (2011) 1351–1371.
[3] F. Sahan, M. Kose, C. Hepokur, D. Karakas, M. Kurtoglu, New azo-azomethine-based transition metal complexes: synthesis, spectroscopy, solid-state structure, density functional theory calculations and anticancer studies, Appl. Organomet. Chem. 33 (7) (2019) e4954.
[4] Y. Xie, S. Zhang, X. Ge, W. Ma, X. He, Y. Zhao, J. Ye, H. Zhang, A. Wang, Z. Liu, Lysosomal-targeted anticancer half-sandwich iridium (III) complexes modified with lonidamine amide derivatives, Appl. Organomet. Chem. 34 (5) (2020) e5589.
[5] N.J. Patel, B.S. Bhatt, M.N. Patel, Heteroleptic N, N-donor pyrazole based Pt (II) and Pd (II) complexes: DNA binding, molecular docking and cytotoxicity studies, Inorganica Chim. Acta 498 (2019) 119130.
[6] W.H. Mahmoud, M. Omar, F.N. Sayed, G.G. Mohamed, Synthesis, characterization, spectroscopic and theoretical studies of transition metal complexes of new nano Schiff base derived from L-histidine and 2-acetylferrocene and evaluation of biological and anticancer activities, Appl. Organomet. Chem. 32 (7) (2018) e4386.
[7] W.-Y. Zhang, S. Banerjee, C. Imberti, G.J. Clarkson, Q. Wang, Q. Zhong, L.S. Young, I. Romero-Canelón, M. Zeng, A. Habtemariam, Strategies for conjugating iridium (III) anticancer complexes to targeting peptides via copper-free click chemistry, Inorganica Chim. Acta 503 (2020) 119396.
[8] S. Şahin-Bölükbaşı, N. Şahin, M.N. Tahir, C. Arıcı, E. Çevik, N. Gürbüz, İ. Özdemir, B.S. Cummings, Novel N-heterocyclic carbene silver (I) complexes: synthesis, structural characterization, and anticancer activity, Inorganica Chim. Acta 486 (2019) 711–718.
[9] E. Cherneva, M. Atanasova, R. Buyukliev, K. Tomovic, Z. Smelcerovic, A. Bakalova, A. Smelcerovic, 3′-Methyl-4-thio-1H-tetrahydropyranspiro-5′-hydantoin platinum complex as a novel potent anticancer agent and xanthine oxidase inhibitor, Arch. Pharm. 353 (7) (2020) e2000039.
[10] M. Buczkowska, A. Bodtke, U. Lindequist, M. Gdaniec, P.J. Bednarski, Cytotoxic and antimicrobial activities of Cu (II), Co (II), Pt (II) and Zn (II) complexes with N, O-chelating heterocyclic carboxylates, Arch. Pharm. 344 (9) (2011) 605–616.
[11] R.S. Kumar, A. Riyasdeen, M. Dinesh, C.P. Paul, S. Srinag, H. Krishnamurthy, S. Arunachalam, M.A. Akbarsha, Cytotoxic property of surfactant–cobalt (III) complexes on a human breast cancer cell line, Arch. Pharm. 344 (7) (2011) 422–430.
[12] A. Bakalova, H. Varbanov, R. Buyukliev, G. Momekov, D. Ivanov, I. Doytchinova, Platinum complexes with 5-methyl-5 (4-pyridyl) hydantoin and its 3-methyl derivatives: synthesis and cytotoxic activity–quantitative structure-activity relationships, Arch. Pharm. 344 (4) (2011) 209–216.
[13] B.K. Keppler, Metal Complexes in Cancer Chemotherapy, Wiley-VCH1993, 2021.
[14] M.K. Sahoo, G. Jaiswal, J. Rana, E. Balaraman, Organo-photoredox catalyzed oxidative dehydrogenation of N-heterocycles, Chemistry 23 (57) (2017) 14167–14172.
[15] G. Cheng, B. Li, C. Wang, H. Zhang, G. Liang, Z. Weng, H. Hao, X. Wang, Z. Liu, M. Dai, Systematic and molecular basis of the antibacterial action of quinoxaline 1, 4-Di-N-oxides against *Escherichia coli*, PLoS ONE 10 (8) (2015) e0136450.
[16] H. Gao, E.F. Yamasaki, K.K. Chan, L.L. Shen, R.M. Snapka, DNA sequence specificity for topoisomerase II poisoning by the quinoxaline anticancer drugs XK469 and CQS, Mol. Pharmacol. 63 (6) (2003) 1382–1388.
[17] J. Javidi, M. Esmaeilpour, Fe3O4@ SiO2–imid–PMAn magnetic porous nanosphere as recyclable catalyst for the green synthesis of quinoxaline derivatives at room temperature and study of their antifungal activities, Mater. Res. Bull. 73 (2016) 409–422.
[18] D. Gedefaw, M. Tessarolo, M. Prosa, M. Bolognesi, P. Henriksson, W. Zhuang, M. Seri, M. Muccini, M.R. Andersson, Induced photodegradation of quinoxaline based copolymers for photovoltaic applications, Sol. Energy Mater. Sol. Cells 144 (2016) 150–158.
[19] V. Desai, S. Desai, S.N. Gaonkar, U. Palyekar, S.D. Joshi, S.K. Dixit, Novel quinoxalinyl chalcone hybrid scaffolds as enoyl ACP reductase inhibitors: synthesis, molecular docking and biological evaluation, Bioorg. Med. Chem. Lett. 27 (10) (2017) 2174–2180.
[20] R. Zamudio-Vázquez, S. Ivanova, M. Moreno, M.I. Hernandez-Alvarez, E. Giralt, A. Bidon-Chanal, A. Zorzano, F. Albericio, J. Tulla-Puche, A new quinoxaline–containing peptide induces apoptosis in cancer cells by autophagy modulation, Chem. Sci. 6 (8) (2015) 4537–4549.

[21] H. Liu, P. Wang, Q. Zhao, Y. Chen, B. Liu, B. Zhang, Q. Zheng, Syntheses, toxicity and biodistribution of CO-releasing molecules containing M (CO) 5 (M= Mo, W and Cr), Appl. Organomet. Chem. 28 (3) (2014) 169–179.
[22] L.K. Wareham, R.K. Poole, M. Tinajero-Trejo, CO-releasing metal carbonyl compounds as antimicrobial agents in the post-antibiotic era, J. Biol. Chem. 290 (31) (2015) 18999–19007.
[23] R.R. Varma, B.H. Pursuwani, E. Suresh, B.S. Bhatt, M.N. Patel, Single crystal, DNA interaction and cytotoxicity studies of rhenium (I) organometallic compounds, J. Mol. Struct. 1200 (2020) 127068.
[24] R.G. Mohamed, F.M. Elantabli, N.H. Helal, S.M. El-Medani, New group 6 metal carbonyl complexes with 4, 5-dimethyl-N, N-bis (pyridine-2-yl-methylene) benzene-1, 2-diimine Schiff base: synthesis, spectral, cyclic voltammetry and biological activity studies, Spectrochim. Acta Part A 141 (2015) 316–326.
[25] B. Machura, R. Kruszynski, M. Jaworska, P. Lodowski, R. Penczek, J. Kusz, Tricarbonyl rhenium complexes of bis (pyrazol-1-yl) methane and bis (3, 5-dimethylpyrazol-1-yl) methane–synthesis, spectroscopic characterization, X-ray structure and DFT calculations, Polyhedron 27 (6) (2008) 1767–1778.
[26] K. Potgieter, P. Mayer, T. Gerber, N. Yumata, E. Hosten, I. Booysen, R. Betz, M. Ismail, B. van Brecht, Rhenium (I) tricarbonyl complexes with multidentate nitrogen-donor derivatives, Polyhedron 49 (1) (2013) 67–73.
[27] P. Zou, S. Yuan, X. Yang, X. Zhai, J. Wang, Chitosan oligosaccharides with degree of polymerization 2–6 induces apoptosis in human colon carcinoma HCT116 cells, Chem. Biol. Interact. 279 (2018) 129–135.
[28] K.P. Thakor, M.V. Lunagariya, B.S. Bhatt, M.N. Patel, Fluorescence and absorption titrations of bio-relevant imidazole based organometallic Pd (II) complexes with DNA: synthesis, characterization, DNA interaction, antimicrobial, cytotoxic and molecular docking studies, J. Inorg. Organomet. Polym. Mater. 29 (2019) 2262–2273.
[29] B.N. Meyer, N.R. Ferrigni, J.E. Putnam, L.B. Jacobsen, D.E. Nichols, J.L. McLaughlin, Brine shrimp: a convenient general bioassay for active plant constituents, Planta Med. 45 (5) (1982) 31–34.
[30] M.N. Patel, B.S. Bhatt, P.A. Dosi, N.V. Amaravady, H.V. Movaliya, Synthesis, spectral investigation and biological interphase of drug-based mixed ligand copper (II) complexes with terpyridines, Appl. Organomet. Chem. 26 (5) (2012) 217–224.
[31] M.N. Patel, P.A. Dosi, B.S. Bhatt, Synthesis, characterization, antibacterial activity and DNA interaction studies of drug-based mixed ligand copper (II) complexes with terpyridines, Med. Chem. Res. 21 (9) (2012) 2723–2733.
[32] F. Loreto, V. Velikova, Isoprene produced by leaves protects the photosynthetic apparatus against ozone damage, quenches ozone products, and reduces lipid peroxidation of cellular membranes, Plant Physiol. 127 (4) (2001) 1781–1787.
[33] R.L. Heath, L. Packer, Photoperoxidation in isolated chloroplasts: I. Kinetics and stoichiometry of fatty acid peroxidation, Arch. Biochem. Biophys. 125 (1) (1968) 189–198.
[34] J.A. Buege, S.D. Aust, Microsomal lipid peroxidation, in: Methods in Enzymology, 52, Elsevier, 1978, pp. 302–310.
[35] M.L. Kopka, C. Yoon, D. Goodsell, P. Pjura, R.E. Dickerson, Binding of an antitumor drug to DNA: netropsin and CGCGAATT-BrC-GCG, J. Mol. Biol. 183 (4) (1985) 553–563.
[36] J.V. Mehta, S.B. Gajera, D.B. Raval, V.R. Thakkar, M.N. Patel, Biological assessment of substituted quinoline based heteroleptic organometallic compounds, Medchemcomm 7 (8) (2016) 1617–1627.
[37] F. Leng, W. Priebe, J.B. Chaires, Ultratight DNA binding of a new bisintercalating anthracycline antibiotic, Biochemistry 37 (7) (1998) 1743–1753.
[38] P.A. Vekariya, P.S. Karia, B.S. Bhatt, M.N. Patel, Spectroscopic and electrochemical study for evaluating DNA interaction activity of 4-(3-halophenyl)-6-(pyridin-2-yl) pyrimidin-2-amine based piano stool Cp* Rh (III) and Ir (III) complexes, Appl. Organomet. Chem. 33 (10) (2019) e5152.
[39] M.R. Green, J. Sambrook, Rapid isolation of yeast DNA, Cold Spring Harb. Protoc. 2018 (6) (2018) 484–485 pdb. prot093542.
[40] M.R. Waterland, T.J. Simpson, K.C. Gordon, A.K. Burrell, Spectroelectrochemical studies and excited-state resonance-Raman spectroscopy of some mononuclear rhenium (I) polypyridyl bridging ligand complexes. Crystal structure determination of tricarbonylchloro [2, 3-di (2-pyridyl) quinoxaline] rhenium (I), J. Chem. Soc., Dalton Trans. 1998 (1) (1998) 185–192 Dalton Transactions.
[41] K. Chanawanno, J.T. Engle, K.X. Le, R.S. Herrick, C.J. Ziegler, The synthesis and pH-dependent behaviour of Re (CO) 3 conjugates with diimine phenolic ligands, Dalton Trans. 42 (37) (2013) 13679–13684.
[42] M. Kaplanis, G. Stamatakis, V.D. Papakonstantinou, M. Paravatou-Petsotas, C.A. Demopoulos, C.A. Mitsopoulou, Re (I) tricarbonyl complex of 1, 10-phenanthroline-5, 6-dione: DNA binding, cytotoxicity, anti-inflammatory and anti-coagulant effects towards platelet activating factor, J. Inorg. Biochem. 135 (2014) 1–9.
[43] R.K. Szilagyi, G. Frenking, Structure and bonding of the isoelectronic hexacarbonyls [Hf (CO) 6] 2-,[Ta (CO) 6]-, W (CO) 6,[Re (CO) 6]+,[Os (CO) 6] 2+, and [Ir (CO) 6] 3+: a theoretical study1, Organometallics 16 (22) (1997) 4807–4815.
[44] G. Balakrishnan, T. Rajendran, K.S. Murugan, M.S. Kumar, V.K. Sivasubramanian, M. Ganesan, A. Mahesh, T. Thirunalasundari, S. Rajagopal, Interaction of rhenium (I) complex carrying long alkyl chain with calf thymus DNA: cytotoxic and cell imaging studies, Inorganica Chim. Acta 434 (2015) 51–59.
[45] I. Aziz, M. Sirajuddin, S. Nadeem, S. Tirmizi, Z. Khan, A. Munir, K. Ullah, B. Farooqi, H. Khan, M. Tahir, Synthesis, crystal structure, antibacterial, cytotoxic, and anticancer activities of new Pd (II) complexes of tri-p-tolyl phosphine with thiones, Russ. J. Gen. Chem. 87 (9) (2017) 2073–2082.
[46] M.N. Patel, C.R. Patel, H.N. Joshi, K.P. Thakor, DNA interaction and cytotoxic activities of square planar platinum (II) complexes with N, S-donor ligands, Spectrochim. Acta Part A 127 (2014) 261–267.
[47] B. Tweedy, Plant extracts with metal ions as potential antimicrobial agents, Phytopathology 55 (1964) 910–914.
[48] L.C.-C. Lee, K.-.K. Leung, K.K.-W. Lo, Recent development of luminescent rhenium (I) tricarbonyl polypyridine complexes as cellular imaging reagents, anticancer drugs, and antibacterial agents, Dalton Trans. 46 (47) (2017) 16357–16380.
[49] W.H. Park, The effects of exogenous H_2O_2 on cell death, reactive oxygen species and glutathione levels in calf pulmonary artery and human umbilical vein endothelial cells, Int. J. Mol. Med. 31 (2) (2013) 471–476.
[50] G. Vilema-Enríquez, A. Arroyo, M. Grijalva, R.I. Amador-Zafra, J. Camacho, Molecular and Cellular Effects of Hydrogen Peroxide on Human Lung Cancer Cells: Potential Therapeutic Implications, Oxidative Medicine and Cellular Longevity, 2016 2016.
[51] P.A. Vekariya, P.S. Karia, J.V. Vaghasiya, S. Soni, E. Suresh, M.N. Patel, Evolution of rhodium (III) and iridium (III) chelates as metallonucleases, Polyhedron 110 (2016) 73–84.
[52] S.S. Mati, S.S. Roy, S. Chall, S. Bhattacharya, S.C. Bhattacharya, Unveiling the groove binding mechanism of a biocompatible naphthalimide-based organoselenocyanate with calf thymus DNA: an “ex vivo” fluorescence imaging application appended by biophysical experiments and molecular docking simulations, J. Phys. Chem. B 117 (47) (2013) 14655–14665.
[53] J.V. Mehta, S.B. Gajera, M.N. Patel, Biological applications of pyrazoline-based half-sandwich ruthenium (III) coordination compounds, J. Biomol. Struct. Dyn. 35 (7) (2017) 1599–1607.
[54] B. Nordén, F. Tjerneld, Structure of methylene blue–DNA complexes studied by linear and circular dichroism spectroscopy, Biopolymers 21 (9) (1982) 1713–1734.
[55] A.K. Patra, T. Bhowmick, S. Roy, S. Ramakumar, A.R. Chakravarty, Copper (II) complexes of L-arginine as netropsin mimics showing DNA cleavage activity in red light, Inorg. Chem. 48 (7) (2009) 2932–2943.
[56] R. Bera, B.K. Sahoo, K.S. Ghosh, S. Dasgupta, Studies on the interaction of isoxazolcurcumin with calf thymus DNA, Int. J. Biol. Macromol. 42 (1) (2008) 14–21.
[57] Y. Gilad, H. Senderowitz, Docking studies on DNA intercalators, J. Chem. Inf. Model. 54 (1) (2013) 96–107.
[58] D. Shao, M. Shi, Q. Zhao, J. Wen, Z. Geng, Z. Wang, Synthesis, crystal structure, DNA binding, cleavage and docking studies of a novel dinuclear Schiff-base copper (II) complex, Z. Anorg. Allg. Chem. 641 (2) (2015) 454–459.
[59] A. Pyle, J. Rehmann, R. Meshoyrer, C. Kumar, N. Turro, J.K. Barton, Mixed-ligand complexes of ruthenium (II): factors governing binding to DNA, J. Am. Chem. Soc. 111 (8) (1989) 3051–3058.